

Aerodynamics of Fan Flow Deflectors for Jet Noise Suppression

Dimitri Papamoschou* and Feng Liu*

University of California, Irvine, Irvine, California 92697-3975

DOI: 10.2514/1.33415

We present a three-dimensional Reynolds-averaged Navier–Stokes investigation of the impact on nozzle aerodynamic performance of deflector vanes used for noise suppression in separate-flow turbofan engines. The vanes are installed in the bypass duct and deflect the bypass plume downward relative to the core plume. This study considers a single pair of vanes, with a NACA 0012 airfoil section, installed in a realistically shaped nozzle operating at static conditions. The vane airfoils are subjected to an externally imposed favorable pressure gradient which delays separation and distorts the pressure distribution around the airfoils. The axial and transverse forces of the system comprising the nozzle walls and the vanes are computed for various vane angles of attack. It is shown that the thrust loss of the bypass stream ranges from 0.04% with the vanes at zero angle of attack to 0.10% for vanes at 8 deg angle of attack. For an entire engine with bypass ratio of 5, the corresponding losses are approximately 0.03 and 0.08%. The vanes have an impact of less than 0.025% on the nozzle flow coefficient.

Nomenclature

C_D	=	drag coefficient
C_L	=	lift coefficient
C_p	=	pressure coefficient
c	=	vane chord length
D	=	drag force
E	=	total internal energy
h	=	vane span
k	=	turbulent kinetic energy
\mathcal{L}	=	lift force
M	=	Mach number
p	=	static pressure
q	=	dynamic pressure
S	=	planform area of vanes
T	=	thrust
t	=	airfoil thickness
u, v, w	=	velocity components
\mathcal{V}	=	volume enclosed by vane
x, y, z	=	Cartesian coordinates
α	=	angle of attack, closure coefficient
β, β^*	=	closure coefficients
γ	=	specific heat ratio
ϵ	=	plume deflection angle
μ_L	=	molecular viscosity
μ_T	=	turbulent viscosity
ρ	=	density
σ^*	=	closure coefficient
τ	=	stress tensor
ω	=	specific dissipation rate

Subscripts

a	=	ambient
e	=	exit
LE	=	vane leading edge
MID	=	vane midchord
TE	=	vane trailing edge

Presented as Paper 0994 at the 43rd Aerospace Sciences Meeting, Reno, NV, 10–13 January 2005; received 13 July 2007; accepted for publication 4 January 2008. Copyright © 2008 by D. Papamoschou and F. Liu. Published by the American Institute of Aeronautics and Astronautics, Inc., with permission. Copies of this paper may be made for personal or internal use, on condition that the copier pay the \$10.00 per-copy fee to the Copyright Clearance Center, Inc., 222 Rosewood Drive, Danvers, MA 01923; include the code 0748-4658/08 \$10.00 in correspondence with the CCC.

*Professor, Department of Mechanical and Aerospace Engineering, Associate Fellow AIAA.

I. Introduction

THE increase in bypass ratio over the last three decades has resulted in a dramatic suppression in the jet noise of turbofan engines. However, this benefit is being offset by an increasing volume of aircraft operations. The worldwide pressure for quieter aircraft is driving the development of advanced nozzle designs that combine noise reduction with aerodynamic efficiency. Today the most successful technique for reducing jet noise from high-bypass engines involves the installation of chevron mixers on the exhaust nozzles [1]. However, the ever increasing demand for quieter engines requires exploration of alternative techniques that could be used by themselves or in conjunction with existing methods.

The recently proposed fan flow deflection (FFD) technology targets suppression of “large-scale” turbulent mixing noise from aircraft engines [2]. Large-scale mixing noise is the most intense noise source in turbulent pressure-matched jets and radiates at angles close to the jet axis. The overarching principle of the FFD method is reduction of the convective Mach number of turbulent eddies that generate intense downward and sideward sound radiation. In a coaxial separate-flow turbofan engine this is achieved by tilting the bypass (secondary) plume by a few degrees downward relative to the core (primary) plume. Mean flow surveys show that the misalignment of the two flows causes a thick, low-speed secondary core on the underside of the high-speed primary flow, especially in the region near the end of the primary potential core which contains the strongest noise sources. The secondary core reduces the convective Mach number of primary eddies, thus hindering their ability to generate sound that travels to the downward acoustic far field.

Tilting of the bypass stream is possible by means of fixed or variable vanes installed near the exit of the bypass duct. Figure 1 depicts the general concept. Subscale experiments at the University of California (U.C.) Irvine have demonstrated significant reductions in perceived noise level [2]. The experiments simulated the shape and flow conditions of realistic exhaust systems at static conditions. Figure 2 shows subscale experimental data on reduction in the overall sound pressure level versus polar angle measured from the jet axis [3]. The nozzle shape and vane installation were the same as those studied in this paper. The noise reduction trends observed in the U.C. Irvine experiments have been confirmed by larger-scale experiments at the NASA John H. Glenn Research Center at bypass ratios 5 and 8 [4]. As with any noise reduction scheme, we need to assess its aerodynamic efficiency. Experimental measurement of jet thrust with accuracy of at least 0.1%, required for meaningful performance evaluation, is very challenging and, as a result, there are very few facilities in the world with such capability. Computation, on the other hand, has the potential to provide accurate estimates of the aerodynamics forces. Importantly, it can also provide physical

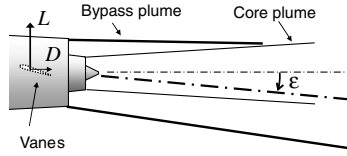


Fig. 1 General concept of fan flow deflection.

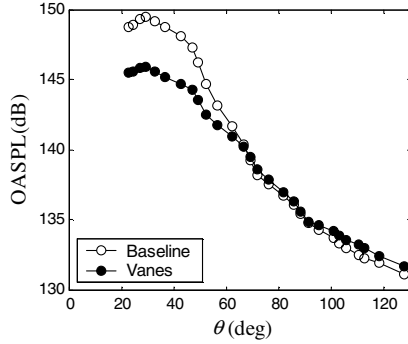


Fig. 2 Overall sound pressure level (OASPL) versus polar angle for nozzle without and with a single pair of vanes at $\alpha = 10$ deg [3].

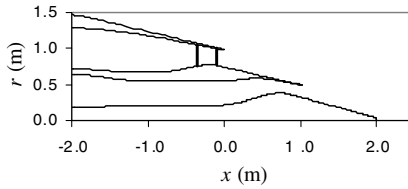


Fig. 3 Radial coordinates of the nozzle showing placement of vanes.

insight into the salient flow physics. This paper describes a computational effort to predict the aerodynamic forces generated by deflector vanes installed inside the bypass duct. The shape of the nozzle approximates that of the separate-flow nozzle tested in the NASA Glenn Research Center [1]. The size of the nozzle corresponds to that of a full-scale engine producing 220 kN of static thrust. We examine a generic placement of a single pair of vanes, illustrated in Fig. 3, with a NACA 0012 airfoil section. Even though the absence of experimental thrust data prevents a direct comparison with the computational fluid dynamics (CFD) data, where possible we compare our CFD prediction on components of the problem with available measurements or with analytical estimates.

II. Computational Approach

A. Numerical Code

The computational fluid dynamics code used here is known as PARCAE and solves the unsteady three-dimensional Reynolds-averaged Navier–Stokes (RANS) equations on structured multiblock grids using a cell centered finite-volume method with artificial dissipation as proposed by Jameson et al. [5]. Residual smoothing is used to increase stability. Information exchange for flow computation on multiblock grids using multiple CPUs is implemented through the message passing interface (MPI) protocol. The RANS equations are solved using the eddy viscosity-type turbulence models. The code contains the Baldwin–Lomax algebraic model and the $k-\omega$ two-equation model of Wilcox [6]. Multigrid convergence acceleration is also available. In this study, only the steady-state solution is obtained because we are interested in the time-averaged features of the flow. Because we may deal with the possibility of separated flow over the vane airfoils, the $k-\omega$ model was chosen because algebraic models become unreliable for separated flows. Next we summarize the main elements of the code.

The governing equations for the unsteady compressible turbulent flow with a two-equation $k-\omega$ turbulence model are expressed as follows:

$$\frac{\partial}{\partial t} \int_{\Omega} \mathbf{W} d\Omega + \oint_{\partial\Omega} (\mathbf{F}_c - \mathbf{F}_d) dS = \int_{\Omega} \mathbf{S} d\Omega \quad (1)$$

The vector \mathbf{W} contains the conservative variables

$$\mathbf{W} = (\rho, \rho u, \rho v, \rho w, \rho E, \rho k, \rho \omega)^T \quad (2)$$

The fluxes consist of the inviscid convective fluxes \mathbf{F}_c and the diffusive fluxes \mathbf{F}_d . For the convective fluxes we include the pressure term

$$\mathbf{F}_c = \begin{Bmatrix} \rho u & \rho v & \rho w \\ \rho u u + p & \rho u v & \rho u w \\ \rho v u & \rho v v + p & \rho v w \\ \rho w u & \rho w v & \rho w w + p \\ \rho E u + p u & \rho E v + p v & \rho E w + p w \\ \rho k u & \rho k v & \rho k w \\ \rho \omega u & \rho \omega v & \rho \omega w \end{Bmatrix} \quad (3)$$

For the diffusive fluxes we have

$$\mathbf{F}_d = \begin{Bmatrix} 0 & 0 & 0 \\ \tau_{xx} & \tau_{xy} & \tau_{xz} \\ \tau_{yx} & \tau_{yy} & \tau_{yz} \\ \tau_{zx} & \tau_{zy} & \tau_{zz} \\ \theta_x & \theta_y & \theta_z \\ \mu^* \frac{\partial k}{\partial x} & \mu^* \frac{\partial k}{\partial y} & \mu^* \frac{\partial k}{\partial z} \\ \mu^* \frac{\partial \omega}{\partial x} & \mu^* \frac{\partial \omega}{\partial y} & \mu^* \frac{\partial \omega}{\partial z} \end{Bmatrix} \quad (4)$$

where

$$\mu^* = \mu_L + \sigma^* \mu_T, \quad \mu_T = \frac{\rho k}{\omega}$$

and

$$\theta_x = u\tau_{xx} + v\tau_{xy} + w\tau_{xz} + \mu^* \frac{\partial k}{\partial x}$$

$$\theta_y = u\tau_{xy} + v\tau_{yy} + w\tau_{yz} + \mu^* \frac{\partial k}{\partial y}$$

$$\theta_z = u\tau_{xz} + v\tau_{yz} + w\tau_{zz} + \mu^* \frac{\partial k}{\partial z}$$

with τ being the stress tensor. The source term is

$$\mathbf{S} = \left(0, 0, 0, 0, 0, \tau_{ij} \frac{\partial u_i}{\partial x_j} - \beta^* \rho \omega k, \frac{\alpha \omega}{k} \tau_{ij} \frac{\partial u_i}{\partial x_j} - \beta \rho \omega^2 \right)^T \quad (5)$$

In the above equations, the closure coefficients were set at $\alpha = 5/9$, $\beta = 3/40$, $\beta^* = 9/100$, and $\sigma^* = 1/2$. The equations are discretized in space by a structured hexahedral grid using a cell centered finite-volume method. The computational domain is decomposed into structured subdivisions. Because within the code each block is considered as a single entity, only flow and turbulence quantities at the block boundaries need to be exchanged. The governing equations are solved explicitly in a coupled manner through a five-stage Runge–Kutta scheme. A time-accurate solution is obtained through a dual-time stepping scheme. Details of the numerical method and implementation of the $k-\omega$ turbulence model can be found in Liu and Zheng [7]. Several acceleration techniques are implemented. Convergence to steady state is increased by local time stepping. Residual smoothing introduced by Jameson and Baker [8] gives the explicit scheme an implicit character and increases the maximum allowable Courant–Friedrichs–Lewy (CFL) number, and thus a larger local time step.

B. Computational Grid

The multiblock grid began four fan diameters upstream of the nozzle exit and ended at the nozzle exit of the bypass duct. The

computational domain did not include the external mixing of the fan-bypass flow with the core jet and the ambient air, which may slightly influence the circumferential and radial distribution of the flow at the exit plane of the fan duct. For a given average pressure condition at the fan-duct exit, however, such influences are minor compared to the large axial as well as circumferential and radial variations of the flow imposed by the internal geometry of the fan duct and the installation of the vanes inside. As we are primarily interested in the major aerodynamic characteristics of the fan deflectors inside the fan duct in this paper, the secondary effect from the external part of the flow is deferred to a future study. Figure 4 shows views of the grid and its topology. Tables 1 and 2 provide the grid sizes for the clean nozzle and the nozzle with vanes, respectively. A symmetric, diametrically opposing pair of vanes was used. Because of this symmetry, only one-half (180 deg) of the nozzle was modeled. For the clean case, only one zone was necessary; however, the computational domain was divided in the axial direction into four blocks of equal cell count to take advantage of PARCAE's parallel processing capability. For each of the cases with vanes installed, a

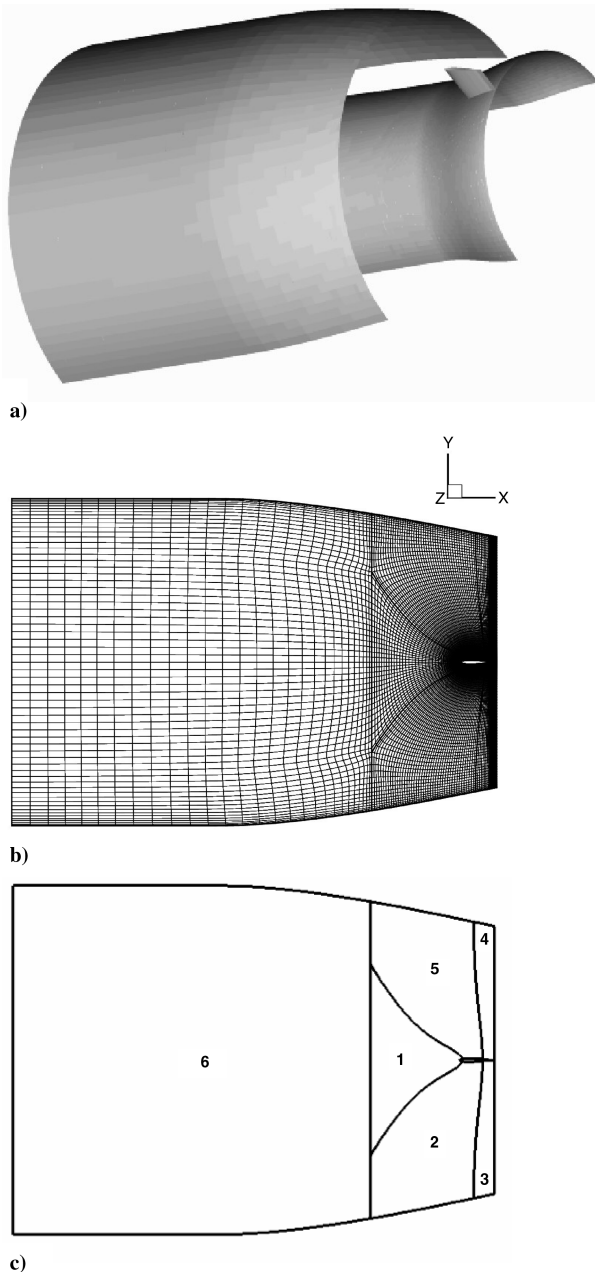


Fig. 4 Computational grid. a) Nozzle and vane surfaces; b) projected view of the grid on a cylindrical surface through the midspan of the vane; c) block topology.

Table 1 Grid for clean nozzle

Zone	Description	Dimensions
1	Inlet block	$33 \times 129 \times 57$
2	Midsection block	$33 \times 129 \times 57$
3	Midsection block	$33 \times 129 \times 57$
4	Exit block	$33 \times 129 \times 57$

Table 2 Grid for nozzle with vane

Zone	Description	Dimensions
1	C grid (front)	$33 \times 113 \times 57$
2	C grid (bottom/front)	$45 \times 129 \times 57$
3	C grid (bottom/exit)	$45 \times 129 \times 57$
4	C grid (top/front)	$45 \times 129 \times 57$
5	C grid (top/exit)	$45 \times 129 \times 57$
6	Inlet grid (upstream)	$29 \times 65 \times 57$

multiblock grid with six zones was constructed. The six zones can be categorized into two larger regions. Zones 1–5 make up the C grid around the vane in the region near the nozzle exit plane. Zone 6 corresponds to the region directly upstream of the C grid that extends to the nozzle inlet plane. Figure 4 shows the computational mesh and details of the multiblock grid for cases with vanes installed.

In each grid, the points near the solid walls were clustered such that $y^+ \approx 1$ was enforced at about the midchord of the airfoil. The solid walls were specified as no-slip adiabatic boundaries. The points near the trailing edge of the vane were also clustered. The same grid size and topology were used for all vane angles of attack. The grid was generated by GridPro (Program Development Company). Convergence to steady state was enforced by requiring a 4-order reduction in the residuals. A grid independence study was performed for the airfoil at zero angle of attack. Computations on successively finer grids were performed to monitor the convergence of the integrated aerodynamic parameters including the lift and drag coefficients on the vanes, the mass flow rate of the fan duct, and the thrust forces. The final grid used consists of 1.52×10^6 grid points on which the changes in the predicted values of the forgoing aerodynamic parameters were within plotting accuracy in all figures presented in this paper. The vane chord length was equal to the exit height of the nozzle, and the vane trailing edge was situated 0.25 chord lengths upstream of the nozzle exit. The area-averaged Mach numbers at the planes of the vane leading edge (LE) and trailing edge (TE), without the vane installed, were $M_{LE} = 0.44$ and $M_{TE} = 0.76$. The midchord Mach number is defined as $M_{MID} = (M_{LE} + M_{TE})/2 = 0.60$. Grids were generated for 5 angles of attack ranging from 0 to 8 deg in increments of 2 deg.

C. Flow and Boundary Conditions

The flow conditions imposed at the inlet and exit were the same for all cases. At the inlet, total pressure, total temperature, and zero flow angle were specified. The inlet total pressure corresponded to a perfectly expanded Mach number of 0.9 of the nozzle exit flow. The total temperature at the inlet was such that the nozzle exit temperature matched the ambient temperature. For subsonic exit flow conditions, the average pressure at the exit plane of the fan duct must be prescribed. In principle, the precise average pressure at the exit plane must be determined from a computation that combines both the internal and the external flowfields. Because we neglect the effect of the external flow, we take the ambient pressure p_a as the average pressure at the exit plane as a first-order approximation. Notice that this same pressure condition is used for both the clean-nozzle configuration without the deflection vanes and that with the vanes and therefore should not significantly impact our comparative study of the aerodynamic characteristics of the vanes. However, radial and circumferential distributions of the pressure as well as other flow variables must be determined from the particular flowfield upstream

of the exit plane of the duct. A rigorous approach is to use the nonreflective characteristic type of boundary conditions such as that by Giles [9]. However, a simpler approach is to maintain the same radial and circumferential gradients of the pressure field at the exit plane as those in the cross plane immediately upstream of the exit plane, while keeping the average of the pressure at the exit plane to be the specified static pressure. This is achieved by first extrapolating the pressure from the cross plane one grid point upstream of the exit plane to the exit plane. Let this tentative pressure distribution be \tilde{p}_e . We then scale \tilde{p}_e by $\int_{A_e} \tilde{p}_e dA / (p_a A_e)$ to obtain static pressure distribution at the exit plane p_e , that is,

$$p_e = \frac{\int_{A_e} \tilde{p}_e dA}{\int_{A_e} \tilde{p}_e dA} p_a \quad (6)$$

After the static pressure at the exit plane has been determined from the above procedure, the other independent flow variables ρ , u , v , and w are extrapolated from inside the computational domain. This method has been found to be an expedient and sufficiently accurate approach for steady internal flow calculations and is widely used in the computation of turbomachinery flows. The Reynolds number was 32×10^6 based on the fan exit diameter, or 3.2×10^6 based on the vane chord length. This corresponds to a fan exit diameter of 1.7 m.

D. Aerodynamic Parameters

We consider a nozzle discharging at static conditions. The nozzle thrust is obtained by integration of the axial momentum and pressure at the nozzle exit,

$$T = \int_{A_e} (\rho_e u_e^2 + p_e - p_a) dA \quad (7)$$

Given the boundary condition Eq. (6), this reduces to

$$T = \int_{A_e} \rho_e u_e^2 dA \quad (8)$$

The overall lift of the nozzle is obtained by integration of the transverse momentum flux at the nozzle exit

$$\mathcal{L} = \int_{A_e} \rho_e v_e u_e dA \quad (9)$$

and, assuming small angles, the overall deflection of the plume is

$$\epsilon = \frac{\mathcal{L}}{T} \quad (10)$$

The thrust and lift forces were also calculated by integration of the pressures and stresses acting on the vanes and on the nozzle walls. The results were identical to those obtained by Eqs. (8) and (9) within computer roundoff error. For the lift and drag of individual components, such as the vane alone or the nozzle walls alone, the pressures and stresses were integrated over the areas of those components.

Perhaps the most important quantity to emerge from this effort is the thrust loss, defined as

$$\Delta T = T - T_{\text{clean}} \quad (11)$$

where subscript “clean” refers to the clean nozzle without vanes.

The airfoil flows studied here are fairly unique in that they are subjected to an *externally imposed favorable pressure gradient*. In other words, because of the convergence of the nozzle, the “freestream” velocity accelerates in the axial direction. Definition of the aerodynamic coefficients becomes problematic as there is no fixed reference condition. Here we make the somewhat arbitrary selection of using as reference the area-averaged conditions in the plane of the vane LE, in the absence of the vane. The pressure coefficient is defined as

$$C_p = \frac{p - p_{LE}}{q_{LE}} \quad (12)$$

the lift coefficient is

$$C_L = \frac{\text{lift}}{q_{LE} S} \quad (13)$$

and the drag coefficient is

$$C_D = \frac{\text{drag}}{q_{LE} S} \quad (14)$$

where q is the dynamic pressure and S is the vane planform area.

III. Results and Discussion

In presenting the aerodynamics of the flow around vanes we will make frequent reference to the flow around a two-dimensional airfoil of the same cross section in an infinite freestream, with $M_\infty = M_{LE} = 0.44$ and the same Reynolds number based on chord length. This information will provide guidance to a designer who wants to use a certain type of airfoil, whose properties in an infinite freestream have been documented, for the internal vanes. As will be seen in Fig. 11, the velocity profile in the duct is uniform enough to allow this analogy. For brevity, we will use the wording “external” for the reference 2-D airfoil, “internal” for the vane alone inside the nozzle, and “system” for the combination of vane and nozzle walls.

We begin with the Mach number isocontours, shown in Fig. 5. For the internal airfoil, these contours were calculated in the midplane of the vane. Because of the accelerating nozzle flow, there are substantial differences between the flowfields of the internal and external airfoils. It is notable that for $\alpha = 8$ deg the external airfoil develops a distinct sonic bubble on the upper surface a short distance past the leading edge. For the internal airfoil, there is no presence of such a bubble. This suggests that the favorable pressure gradient delays the onset of sonic flow and its adverse effects on aerodynamic performance.

The pressure coefficient C_p on the vane surface is plotted in Fig. 6. We notice that for $\alpha > 0$ the C_p near the leading edge on the internal airfoil does not become as negative as that of the external airfoil, which is consistent with the Mach number contours of Fig. 5. In fact, C_p on the upper surface of the internal airfoil is reminiscent of that on a supercritical airfoil. Again this indicates that the externally imposed negative pressure gradient delays wave-drag effects. Even though the C_p distributions for the internal and external airfoils are very different, the areas enclosed by these distributions are equal to within a few percent. Note that the lift coefficient is proportional to the area enclosed by the upper and lower C_p distributions.

It is important to also examine the pressure distribution on the nozzle walls, especially the differences caused by insertion of the vane. To obtain an overall assessment, we examine the axial distribution of the circumferentially averaged pressure and define a pressure coefficient as per Eq. (12). Figure 7 plots the difference in nozzle wall C_p with and without the vane at $\alpha = 0$ deg. Insertion of the vane reduces slightly the pressure on both nozzle walls due to the reduced cross-sectional area of the duct. On the outer nozzle wall, which has a significant inclination (Fig. 3), the pressure drop creates an axial force in the direction of positive thrust. The implication of this phenomenon on the force balance of the entire nozzle will become evident later.

Figure 8 plots the lift curves for the external airfoil, the internal airfoil, and the system. We note that all the curves are very similar. The lift curve slope of the internal airfoil is slightly larger than that of the external airfoil. When we include the lift contribution of the nozzle surfaces the lift curve slope declines slightly, indicating a mild cancellation effect. The lift curve slope for the system is 0.13 deg^{-1} , which is close to the theoretical value for a 2-D airfoil.

We now turn our attention to the drag coefficient C_D . For the external airfoil and for the vane-alone internal airfoil, the drag is calculated by surface integration of pressures and stresses. When we consider the system (vane plus nozzle), the drag is based on the thrust

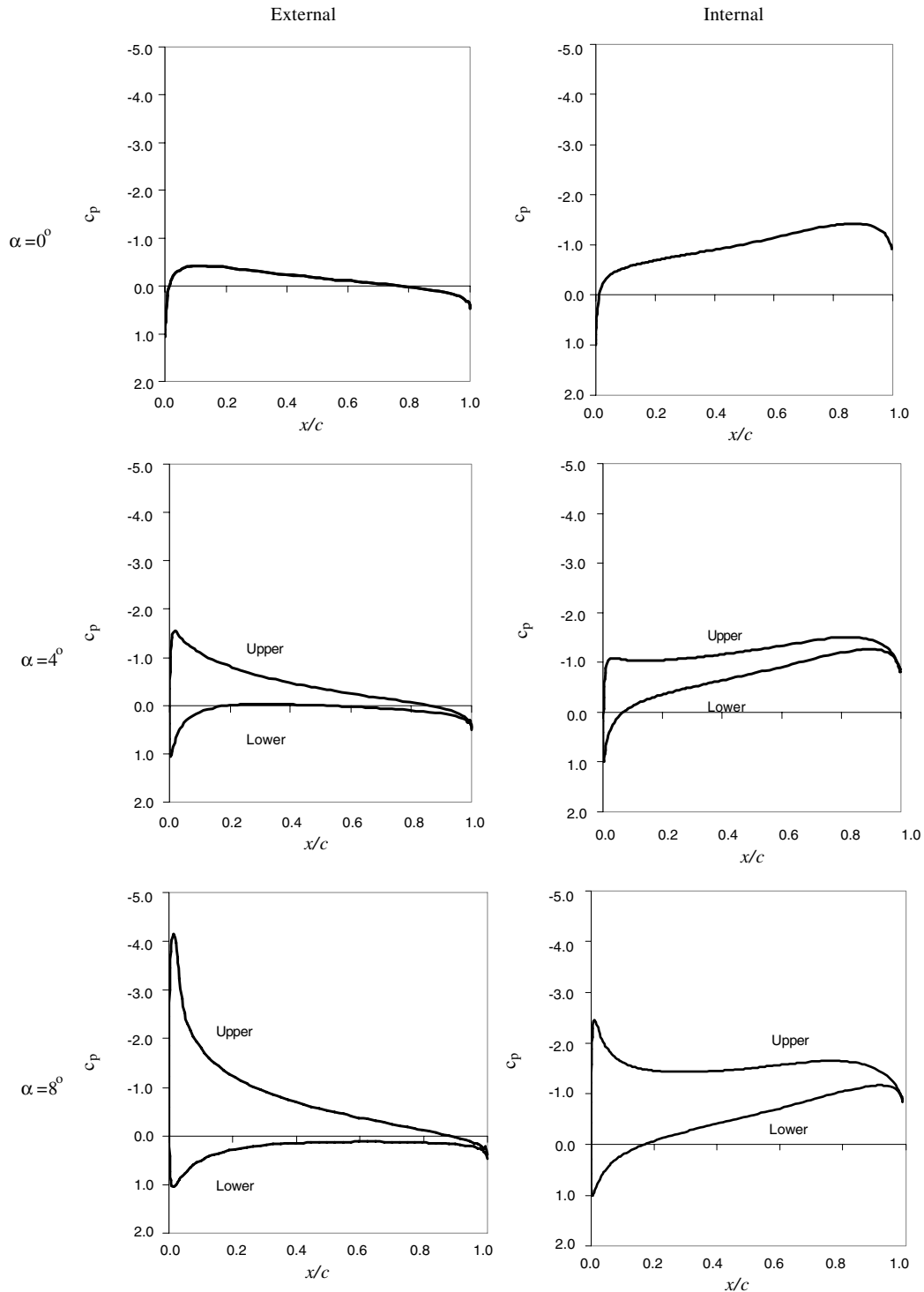


Fig. 6 Pressure coefficient for external airfoil (left column) and midplane of internal vane (right column) for $\alpha = 0$ deg, 4, and 8 deg.

force that is equal and opposite to D_h . In other words, the potential-flow processes in the nozzle should produce zero net drag. The net drag (system drag) computed is the result of entropy generation due to viscous and possibly wave phenomena caused by the vane airfoil.

The system drag coefficient still seems large compared to the drag coefficient of the external airfoil (0.024 versus 0.0076 at zero angle of attack). Recall, however, that we made a rather arbitrary decision to base the aerodynamic coefficients on the conditions of the leading edge ($M_{LE} = 0.44$). If we select the midchord conditions ($M_{MID} = 0.6$) for reference, the drag coefficients of the external airfoil and of the system become comparable, especially for high angle of attack, as shown in Fig. 10. In this figure, the $C_D - \alpha$ relation for the external airfoil matches very well experimental data by Harris

[12] for the NACA 0012 airfoil at the same Mach number (0.6) and similar Reynolds number (3×10^6).

We must also consider vane-wall interference effects that can generate secondary losses. Roach and Turner [13] proposed the following relation for the drag increment due to secondary losses of airfoil-shaped support struts in gas turbine passages:

$$\Delta C_D = \frac{1.9}{\sqrt{1 - M^2}} \frac{t}{c} \frac{\delta^*}{h} \quad (18)$$

where M is the Mach number, t/c is the thickness-to-chord ratio, h is the span of the strut, and δ^* the average boundary layer displacement thickness on the two walls supporting the strut. In our case, the

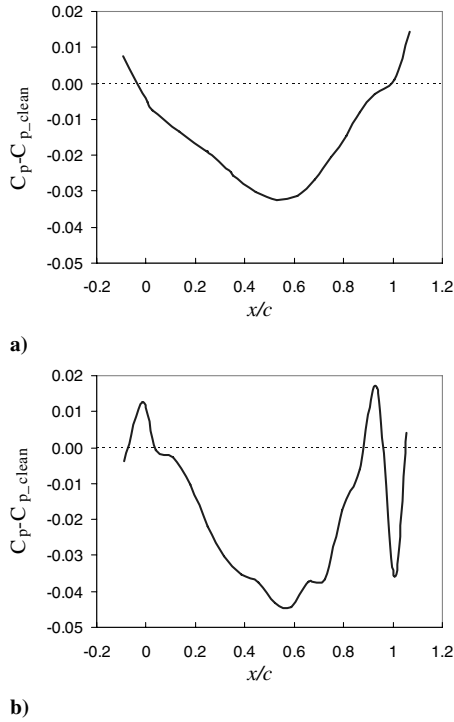


Fig. 7 Coefficient of circumferentially averaged pressure on nozzle walls. Plotted is the difference between the case with the vane at $\alpha = 0$ deg and the clean case. a) Inner wall; b) outer wall. x is referenced to the axial position of the vane leading edge.

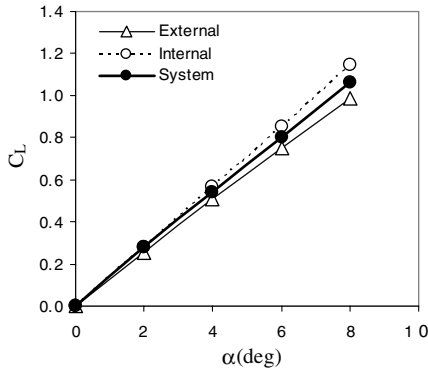


Fig. 8 Lift coefficient versus vane angle of attack. Reference conditions at vane leading edge.

velocity profile approaching the vane, plotted in Fig. 11, has an average displacement thickness of 3 mm. Applying Eq. (18) to our vane, we obtain an increment $\Delta C_D = 0.0039$. Considering the $\alpha = 0$ deg case, if we add this increment to the drag coefficient of the external airfoil at $M = 0.60$ ($C_D = 0.0087$), the total drag coefficient becomes 0.0126 which is close to the system value of 0.0123 shown in Fig. 10. Secondary losses can be mitigated by adding small fillets at the junction of the vanes with the nozzle walls [14].

Figure 12 plots the overall deflection angle of the bypass plume, computed using Eq. (10). The deflection angles are small, less than 1.2 deg, and in line with the deflections measured experimentally in similar nozzles [3]. Given the result of Fig. 8, the deflection angle is now easily predicted theoretically because the lift in Eq. (13) can be obtained directly from the $C_L - \alpha$ relation of the airfoil used. The deficit in nozzle mass flux is plotted in Fig. 13. Insertion of the vanes at $\alpha = 0$ deg has insignificant impact on the mass flow rate. At the highest angle of attack, the mass flux deficit is 0.022%. The figure also shows the theoretical prediction based on the deflection angle,

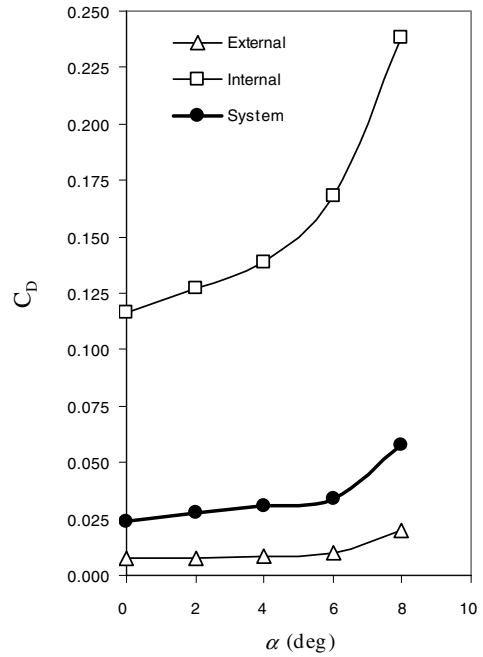


Fig. 9 Drag coefficient versus vane angle of attack. Reference conditions at vane leading edge.

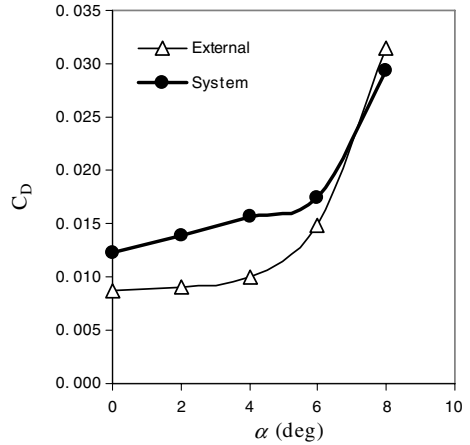


Fig. 10 Drag coefficient versus vane angle of attack for external airfoil and for system. Reference conditions at vane midchord.

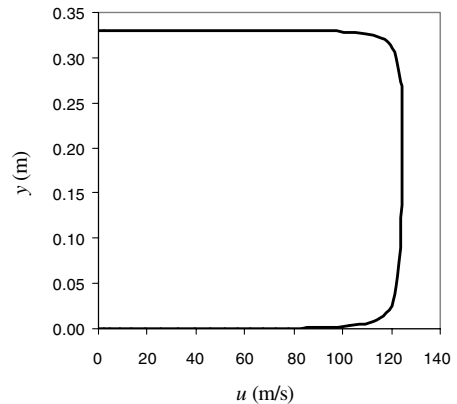


Fig. 11 Velocity profile in the duct one-half chord length ahead of vane.

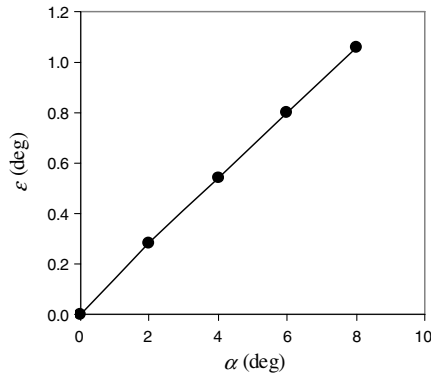


Fig. 12 Plume deflection angle versus vane angle of attack.

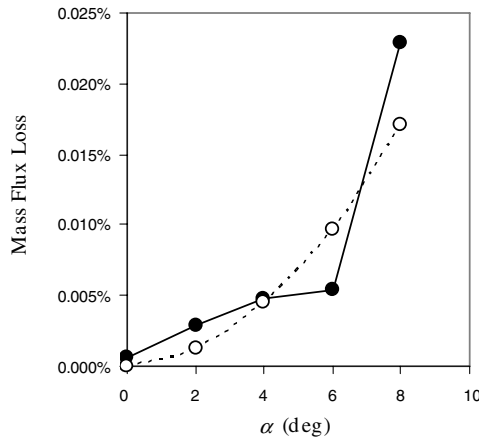


Fig. 13 Percent mass flux deficit versus vane angle of attack. Solid symbols: computation; open symbols: theory based on the cosine of the plume deflection angle.

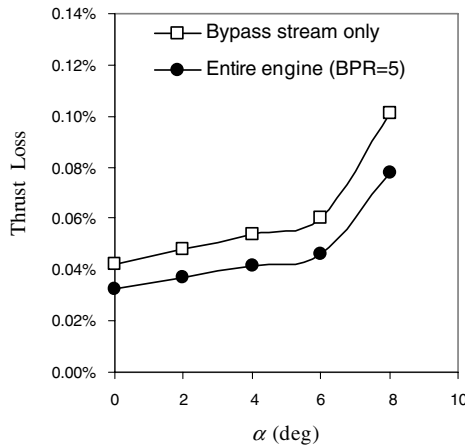


Fig. 14 Percent thrust loss versus vane angle of attack.

assuming that the velocity profile at the exit is uniform in u and v . In that case, the mass flux deficit is $1 - \cos \epsilon$, with ϵ given by Fig. 12. The computational result is in general agreement with the theoretical prediction.

The thrust loss versus vane angle of attack is plotted in Fig. 14. Two plots are shown, one for the bypass stream alone (the subject of this computation) and the other for the entire engine. The thrust loss for the bypass stream starts at 0.04% with the vanes at $\alpha = 0$ deg and reaches 0.10% for $\alpha = 8$ deg. For an engine with bypass ratio of 5, the bypass stream produces about 77% of the total thrust, so the losses for the entire engine become 0.033% at $\alpha = 0$ deg and 0.078% at $\alpha = 8$ deg. These losses appear acceptable from a performance point of view.

IV. Conclusions

We examined computationally the flowfield arising from the installation of airfoil-type vanes inside the bypass duct of a turbofan engine. The function of the vanes is to deflect the bypass plume for the purpose of noise reduction. This is a unique flowfield where an airfoil is subjected to an externally imposed favorable pressure gradient. The pressure gradient is shown to delay the onset of sonic flow on the airfoil. The lift curve slope matches that of the same airfoil in an infinite freestream when the lift coefficient is based on the Mach number in the clean duct at the axial position of the leading edge of the vane. The lift of the entire system (comprising the nozzle walls and the vanes) is practically the same as the lift of the isolated vane. The drag coefficient of the isolated vane is large due to the axial pressure gradient acting across the airfoil length which creates a buoyancylike effect. This effect is counteracted by a reduced pressure on the internal nozzle walls, yielding a system drag coefficient comparable to that of an external airfoil when the reference Mach number is the Mach number in the clean duct at the vane midchord. This is an important result because it allows one to get a preliminary estimate of the thrust loss simply by knowing the drag characteristics of the isolated vane airfoil. The thrust loss of the bypass stream ranges from 0.04% with the vanes at zero angle of attack to 0.10% for vanes at 8 deg angle of attack. For an entire engine with bypass ratio of 5, the corresponding losses are approximately 0.03 and 0.08%. The vanes have an impact of less than 0.025% on the nozzle flow coefficient.

The computation ended at the fan exit plane and did not include the core cowling and the core flow present in a turbofan engine. Extension of the computation to include these components is the subject of an ongoing effort. We expect, however, that the downstream phenomena will have little impact on the fundamental results presented here, namely, that the thrust loss and plume deflection angle are consistent with those one would estimate by looking at the aerodynamic properties of the vane airfoil. The viscous wake of the vane was computed here only up to the fan exit plane. Its effect on thrust was captured by Eq. (7). Further downstream, the wake will cause a slight redistribution of velocity on the core cowling. Although this may have some impact on thrust (positive or negative), we expect it to be of much lesser magnitude than the drag force of the vane. In many engine designs the core stream exhausts well downstream (as much as half a fan diameter) of the bypass stream, in which case the influence of the core stream on the flow processes inside the bypass duct should be minimal.

Acknowledgments

This work was supported by the NASA John H. Glenn Research Center at Lewis Field, Grant NAG-3-2345 (Grant Monitors, K. Zaman and J. Bridges). We thank Tadashi Murayama for performing the computations and Mani Sadeghi for his guidance. The method and system of noise suppression via deflection of the bypass and/or core streams is proprietary to the University of California, U.S. Patent No. 7,293,401.

References

- [1] Saiyed, N. H., Mikkelsen, K. L., and Bridges, J. E., "Acoustics and Thrust of Quiet Separate-Flow High-Bypass-Ratio Engines," *AIAA Journal*, Vol. 41, No. 3, 2003, pp. 372-378.
- [2] Papamoschou, D., "Fan Flow Deflection in Simulated Turbofan Exhaust," *AIAA Journal*, Vol. 44, No. 12, 2006, pp. 3088-3097. doi:10.2514/1.22552
- [3] Papamoschou, D., and Shupe, R. S., "Effect of Nozzle Geometry on Jet Noise Reduction Using Fan Flow Deflectors," *AIAA Paper 2006-2707*, May 2006.
- [4] Zaman, K., Bridges, J., and Papamoschou, D., "Offset Stream Technology—Comparison of Results from UCI and GRC," *AIAA Paper 2007-0438*, Jan. 2007.
- [5] Jameson, A., Schmitt, W., and Turkel, E., "Numerical Solutions of the Euler Equations by Finite Volume Methods Using Runge-Kutta Time Stepping Schemes," *AIAA Paper 81-1259*, Jan. 1981.

- [6] Wilcox, D. C., "Reassessment of the Scale-Determining Equation for Advanced Turbulence Models," *AIAA Journal*, Vol. 26, No. 11, 1988, pp. 1299–1310.
- [7] Liu, F., and Zheng, X., "A Strongly Coupled Time-Marching Method for Solving the Navier-Stokes and $k-\omega$ Turbulence Model Equations with Multigrid," *Journal of Computational Physics*, Vol. 128, No. 2, 1996, pp. 289–300.
doi:10.1006/jcph.1996.0211
- [8] Jameson, A., and Baker, T. J., "Improvements to the Aircraft Euler Method," AIAA Paper 87-0452, Jan. 1987.
- [9] Giles, M. B., "Non-Reflecting Boundary Conditions for the Unsteady Euler Equations," Massachusetts Institute of Technology, Technical Rept. CFDL-TR-88-1, 1988.
- [10] McCroskey, W. J., "A Critical Assessment of Wind Tunnel Results for the NACA 0012 Airfoil," NASA TM 100019, Oct. 1987.
- [11] Jacobs, E. N., Ward, K. E., and Pinkerton, R. M., "The Characteristics of 78 Related Airfoil Sections from Tests in the Variable-Density Wind Tunnel," NACA, Rept. 460, 1933.
- [12] Harris, C. D., "Two-Dimensional Aerodynamic Characteristics of the NACA 0012 Airfoil in the Langley 8-Foot Transonic Pressure Tunnel," NASA TM 81927, April 1981.
- [13] Roach, P. E., and Turner, J. T., "Secondary Loss Generation by Gas Turbine Support Struts," *International Journal of Heat and Fluid Flow*, Vol. 6, No. 2, June 1985, pp. 79–88.
doi:10.1016/0142-727X(85)90039-6
- [14] Simpson, R. L., "Junction Flows," *Annual Review of Fluid Mechanics*, Vol. 33, Jan. 2001, pp. 415–443.
doi:10.1146/annurev.fluid.33.1.415

J. Oefelein
Associate Editor